JPhys Materials

PAPER • OPEN ACCESS

Asymmetric nanoparticle oxidation observed *in-situ* by the evolution of diffraction contrast

To cite this article: Agus R Poerwoprajitno *et al* 2023 *J. Phys. Mater.* **6** 045013

Journal of Physics: Materials

PAPER

Asymmetric nanoparticle oxidation observed *in-situ* by the evolution of diffraction contrast

Agus R Poerwoprajitno[1], Nitish Baradwaj[2], Manish Kumar Singh[3,4], C Barry Carter[1], Dale L Huber[1], Rajiv Kalia[2] and John Watt[3,*]

[1] Center for Integrated Nanotechnologies, Sandia National Laboratories, Albuquerque, NM 87123, United States of America
[2] Collaboratory for Advanced Computing and Simulations, Department of Physics and Astronomy, Department of Computer Science, Department of Chemical Engineering and Materials Science, Department of Biological Sciences, University of Southern California, Los Angeles, CA 90089-0242, United States of America
[3] Center for Integrated Nanotechnologies, Los Alamos National Laboratory, Los Alamos, NM 87545, United States of America
[4] Current address: Department of Physics, University of Allahabad, Prayagraj, 211002 UP, India
[*] Author to whom any correspondence should be addressed.

E-mail: watt@lanl.gov

Keywords: *in-situ*, environmental TEM, oxidation, iron oxide nanoparticles, Ashby-Brown contrast

Supplementary material for this article is available online

OPEN ACCESS

RECEIVED
24 July 2023

REVISED
11 September 2023

ACCEPTED FOR PUBLICATION
11 October 2023

PUBLISHED
19 October 2023

Abstract

The use of transmission electron microscopy (TEM) to observe real-time structural and compositional changes has proven to be a valuable tool for understanding the dynamic behavior of nanomaterials. However, identifying the nanoparticles of interest typically require an obvious change in position, size, or structure, as compositional changes may not be noticeable during the experiment. Oxidation or reduction can often result in subtle volume changes only, so elucidating mechanisms in real-time requires atomic-scale resolution or *in-situ* electron energy loss spectroscopy, which may not be widely accessible. Here, by monitoring the evolution of diffraction contrast, we can observe both structural and compositional changes in iron oxide nanoparticles, specifically the oxidation from a wüstite-magnetite ($FeO@Fe_3O_4$) core–shell nanoparticle to single crystalline magnetite, Fe_3O_4 nanoparticle. The *in-situ* TEM images reveal a distinctive light and dark contrast known as the 'Ashby-Brown contrast', which is a result of coherent strain across the core–shell interface. As the nanoparticles fully oxidize to Fe_3O_4, the diffraction contrast evolves and then disappears completely, which is then confirmed by modeling and simulation of TEM images. This represents a new, simplified approach to tracking the oxidation or reduction mechanisms of nanoparticles using *in-situ* TEM experiments.

1. Introduction

Transmission electron microscopy (TEM) is a powerful tool for the real time observation of structural and compositional changes in nanomaterials and has been employed widely in heterogeneous catalysis and for the tracking of dynamical evolution of nanostructures, under controlled atmospheric conditions [1–4]. When coupled with aberration correction, TEM performed in bright-field conditions can allow for real-time tracking of atomic movement and facet reconstruction at exposed crystalline surfaces to provide information on nanoparticle evolution with unprecedented temporal and spatial resolution. This has been helped significantly by the development of next-generation direct electron detection cameras that can image at incredibly high speeds and low electron dose rates [5–9]. Further, the increased field of view in such cameras increases the chances of detecting and tracking the dynamical evolution of a nanoparticle of interest. Although atomic-scale information is captured in real time it can typically require post-experimental processing such as drift correction, frame integration and denoising to increase the signal to noise ratio and be observable. Therefore, the tracking of a macroscopical structural event such as surface reconstruction, particle movement (i.e. along a substrate), or particle growth is typically used to identify the region of interest for high resolution observation and analysis. While this is a reasonable approach for many

experiments, nanomaterials that experience subtle structural, crystallographic, or compositional changes can be difficult to identify in bright field TEM, especially given the often-present drift issue. Furthermore, unless the microscope is equipped with *in-situ* electron energy loss spectroscopy (EELS), observing changes in oxidation state is not feasible.

In the present study, we track the evolution of diffraction contrast as an effective identifier of structural and compositional changes during an *in-situ* TEM experiment. When a small spherical inclusion is included in a thin film matrix and there is coherent strain across the interface the TEM image can be dominated by strain-field contrast [10, 11]. Ashby and Brown first observed this contrast phenomenon under a two-beam weak field imaging condition in the TEM. When imaged under a two-beam condition the contrast appears as a pair of lobes approximately symmetrical across a 'line of no contrast'. The line of no contrast is aligned with the image of the particle perpendicular to the active **g** vector [12]. The two-fold symmetry of the contrast is not due to two-fold symmetry of the particle itself, rather it is associated with the principal diffracting plane causing the contrast. When imaged under ideal and calibrated conditions the contrast can be used to measure the coherent strain-field, if no misfit dislocations are present [10]. Ashby-Brown contrast has been observed in Au@Pd core–shell nanocubes, with a lattice mismatch of 4.6%, and CdSe@CdS core–shell nanoparticles, with a lattice mismatch of 4.4% [13, 14].

Iron oxide nanoparticles are ideal nanomaterials for studying the evolution of structural and compositional changes since they can exhibit different oxidation states within a single nanoparticle, e.g. in wüstite-magnetite ($FeO@Fe_3O_4$) core–shell nanoparticles. The lattice mismatch between FeO and Fe_3O_4 has been theoretically and experimentally shown to range from approximately 2.3%–4.6%, falling within the range required for coherent strain conditions [15]. Elucidating the mechanisms of oxidation for iron oxide nanoparticles is an important problem as their magnetic properties depend on their crystal structure, and the formation of defects during oxidation can significantly affect their performance [16]. For example, it has been shown that the presence of antiphase boundaries can decrease the saturation magnetization (M_{sat}) by up to 50%, even in nanoparticles of the same size and overall composition [17].

In this study, we observe the dynamic evolution of Ashby-Brown contrast during the *in-situ* oxidation process of $FeO@Fe_3O_4$ core–shell nanoparticles, leading to the formation of single-crystalline Fe_3O_4 nanoparticles. Through experimental, atomic modeling and simulation of TEM images, we establish a correlation between the progression of light and dark contrast and the corresponding structural and compositional changes. We therefore show that diffraction contrast can be used as an effective identifier of nanoparticle transformations *in-situ*.

2. Methods

2.1. Sample preparation

$FeO@Fe_3O_4$ nanoparticles were prepared by first synthesizing FeO nanoparticles, following a previously reported synthesis, and then letting the surface oxidize passively [18]. To synthesize FeO nanoparticles 1.34 g of $Fe(acac)_3$ (Aldrich, 97%) was combined with 20 ml of dried and degassed oleic acid (Aldrich, 90%) in a 50 ml flask held in a molten metal heating bath. A constant flow of dry N_2 gas was maintained at 10 sccm over the reaction solution. The temperature was then increased to 380 °C where it was held for 4 h. The FeO nanoparticles were stored in their crude reaction solution in the freezer inside the N_2 glovebox, to prevent uncontrolled oxidation. To begin the *in-situ* experiment the FeO nanoparticles were removed from a N_2 glove box and washed with several washing steps using degassed isopropanol and hexanes with centrifugation, to remove excess organic capping ligands. This caused partial oxidation of the nanoparticle surface, resulting in $FeO@Fe_3O_4$ core–shell nanoparticles. A 4 μl aliquot of the $FeO@Fe_3O_4$ core–shell nanoparticles in hexanes was then dropcast onto a Protochips Heating Chip (E-FHDC-ENV-10) and then promptly inserted into the high vacuum of the TEM to prevent any further uncontrolled oxidation.

2.2. *In-situ* analysis

High-resolution TEM (HRTEM) imaging was performed on a FEI Titan environmental TEM (ETEM) with Image Cs corrector operating at 300 keV, equipped with a Gatan K3-IS direct detection camera and Protochips Aduro heating holder and custom gas-delivery cart. The $FeO@Fe_3O_4$ core–shell nanoparticles were then imaged in bright-field conditions with a cumulative e^- dose of 3000 e^- Å^{-2} with no change, indicating there are no appreciable effects from the e^- beam. Oxygen (O_2) gas flow was then set to 10 sccm and pressure controlled to 100 torr at the delivery point to the ETEM. The leak valves were adjusted until a steady column pressure of 2.5 mbar O_2 was achieved. No further oxidation was observed under these conditions at room temperature.

The sample temperature was then increased at a ramp rate of 0.33 °C s^{-1} to minimize the drifting until it reached 175 °C, at which point the column valves were opened and the sample exposed to the e- beam at a

dose rate of 10 e^- $Å^{-2}$ s^{-1}. *In-situ* dataset collection was started once the temperature reached 220 °C (using the 5 s lookback feature) and stopped once complete oxidation was observed at a temperature of 265 °C. Data was recorded at 25 fps using the full field of view of the K3-IS camera (5760 × 4092 pixels).

To increase signal to noise ratio 10 frames of the *in-situ* dataset were summed and aligned, then the region of interest was systematically reduced to isolate and track a single FeO@Fe_3O_4 nanoparticle oriented close to the [110]. All manipulation of the *in-situ* data was performed using the *In-Situ* Editor of Gatan DigitalMicrograph. A final video was then exported at 20 fps, sped up by 16× and compressed for ease of data handling and viewing using a common video editor. To measure the contrast profiles each image was loaded into ImageJ and a vertical contrast profile extracted using the Profile tool. The plots were then smoothed in Origin using Adjacent Averaging with Weight Average and a Reflect boundary condition.

2.3. FeO@Fe_3O_4 core–shell nanoparticle models

To create a model of the core–shell system, we first create a spherical Fe_3O_4 nanoparticle with a diameter of 10 nm. For the uniform system, a spherical void of diameter 8 nm was carved out. To create the low and high skew systems, the void center was moved to 0.5 and 0.25 of the void radius along the *y*-axis. The void diameters were also reduced from 8 nm to 5 and 3 nm for the low- and high-skew systems, respectively. After creating the voids, a FeO nanoparticle was created from the FeO unit cell. The radius of the FeO nanoparticle was less than that of the void by 1%. This was done to ensure relaxation in the interlayer region during conjugate gradient. Fe_3O_4 has a spinel structure and the *Fd*-3*m* space group. FeO_4 tetrahedra are formed when Fe^{2+} are bonded to four O^{2-} ions. The corners of the tetrahedra are shared with 12 FeO_6 octahedra. The unit cell is cubic with a lattice constant of 8.44 Å which results in a unit cell volume of 602.62 $Å^3$. FeO is a rock salt crystal structure in which Fe^{2+} is bonded to six O^{2-} ions. This leads to a formation of FeO_6 octahedra. The lattice constant of FeO is 4.26 Å with a unit cell volume of 77.44 $Å^3$. (However, a more appropriate comparison is to 8 cells of FeO, which equal a volume of 619.52 $Å^3$). The entire system was placed in the center of a 20 nm^3 box and periodic boundary conditions were applied in all the three directions. This creates a standalone nanoparticle which was then thermalized in molecular dynamics simulation.

We used a reactive (ReaxFF) forcefield for the simulations [19]. The reactive forcefield consists of both valence and non-valence interactions. The ReaxFF potential energy consists of the following terms:

$E_{\mathrm{ReaxFF}} = E_{\mathrm{bond}} + E_{\mathrm{lp}} + E_{\mathrm{over}} + E_{\mathrm{under}} + E_{\mathrm{val}} + E_{\mathrm{pen}} + E_{\mathrm{coa}} + E_{\mathrm{tors}} + E_{\mathrm{conj}} + E_{\mathrm{hbond}} + E_{\mathrm{vdw}} + E_{\mathrm{coul}}$. The non-covalent interactions include E_{vdw} and E_{coul}, both of which are screened by a taper function. The charges in ReaxFF are quantified by electronegativity equalization method. The initial forcefield was developed by Kubicki and co-workers [20]. The forcefield describes the interaction of α FeOOH (Geothite) and water. We used this forcefield as the starting point to train a Reax forcefield for our simulation. DFT based calculations of energy and lattice constant were carried out on both FeO and Fe_3O_4 structures and the two and three body terms were updated. We used VASP to carry out our DFT calculations. Generalized gradient approximation GGA-PBE were used with a cutoff of 500 eV [21].

2.4. Image simulation

Atomic-resolution phase-contrast image simulations are carried using the multislice algorithm within the Java-EMS (JEMS) program [22]. Multislice simulations have been performed to generate the thickness-defocus maps of the FeO embedded in Fe_3O_4 matrix nanoparticle structures along [110] direction. These nanoparticles structures are generated by a customized protocol with FeO insertions in Fe_3O_4 with (i) uniform strain (ii) low skewed (iii) high skewed and (iv) pure Fe_3O_4. The simulated images have been generated for a defocus window of −20 nm to −40 nm of the objective lens and in the thickness raging from ∼25 nm to 35 nm. Simulated images of a single nanoparticle are presented with a thickness of ∼25 nm and defocus values of −35 nm. They match well with experimentally observed high-resolution phase-contrast images of the nanoparticles. During the recording of the HRTEM images in the aberration-corrected TEM, the defocus value of the objective-lens system was maintained at approx. −25 nm, while the fine focus control was achieved with a piezo-controlled goniometer-stage movement with nanometer precession. However, the simulation is performed with defocus window ranging −20 to −40 nm to accommodate any deviation during recording of the images.

3. Results and discussion

The FeO nanoparticles were synthesized using a previously reported thermal decomposition method and possessed an average size of 21.1 nm with a size distribution of 6.3% (figure S1) [18]. The nanoparticles are partially oxidized to form FeO@Fe_3O_4 core–shell during TEM sample preparation. They were then dropcast on a Protochips *in-situ*-heating chip and loaded into the ETEM in a Protochips Aduro heating holder. The sample was first imaged with a high e^- dose, with no observable changes, indicating the beam-sample

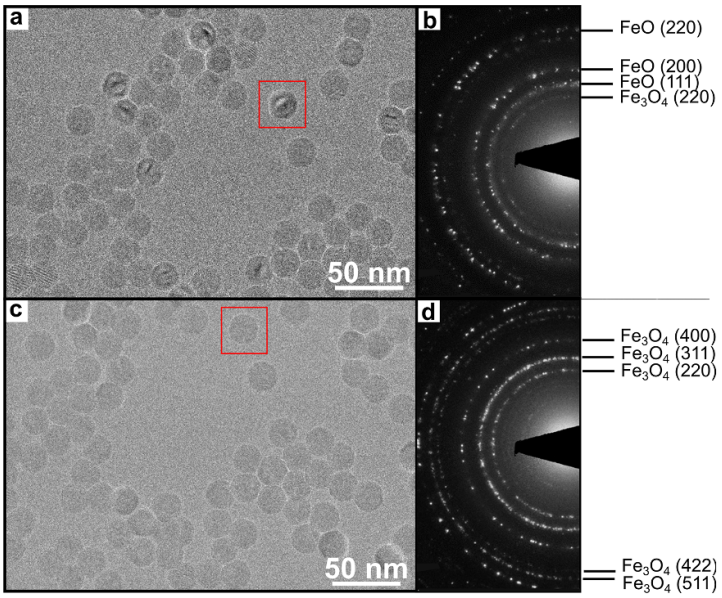

Figure 1. TEM (a) and SAD (b) images of FeO@Fe_3O_4 core–shell nanoparticles taken at t_0 along with images of fully oxidized magnetite (Fe_3O_4) nanoparticles taken at t_f (c) and (d). The Fe_3O_4 (220) ring is faintly visible in (b) indicating the presence of a thin magnetite shell at t_0, which increases in intensity after oxidation (d). The individual nanoparticle tracked and aligned for *in-situ* observation is highlighted in red.

interactions were negligible. Then, O_2 gas was introduced into the column until a steady pressure of 2.5 mbar was achieved. The sample was then heated at 0.33 °C s^{-1} and recording of the *in-situ* dataset was started at the first observable change to the nanoparticles at 220 °C (t_0). TEM images were taken at an *e*- dose of 10 e^- $Å^{-2}$ s^{-1} and 25 frames per second (fps) using the Gatan K3-IS camera (figures S2 and S3, SI). Recording of the *in-situ* dataset was stopped following complete oxidation of the nanoparticles once the temperature reached 265 °C (t_f).

Figure 1(a) shows a TEM image of an ensemble of FeO@Fe_3O_4 core–shell nanoparticles at t_0, before the introduction of O_2 gas. To increase signal to noise ratio and contrast 10 frames of the *in-situ* dataset were summed and aligned using gatan digital micrograph (GMS). Several nanoparticles are oriented to show parallel alternating light and dark diffraction contrast, so called 'Ashby-Brown' contrast [10, 23]. This diffraction contrast is attributed to a local deformation of the crystal lattice and coherent strain across the interface of FeO and Fe_3O_4 and indicates a core–shell structure [10, 14].

Figure 1(b) shows a selected area diffraction (SAD) pattern of FeO@Fe_3O_4 core–shell nanoparticles at t_0. At t_0 we identify rings corresponding to the (111), (200), and (220) reflections of FeO. There is also a weak Fe_3O_4 (220) reflection emerging from the thin shell created by surface oxidation during sample preparation. FeO has a rock-salt-type structure where O^{2-} anions are arranged in *fcc* closed-packed T_h sites and Fe^{2+} ions occupy the O_h sites. The Fe_3O_4 (220) diffraction line is associated with the cations ordered in T_h sites characteristic of spinels and confirms the presence of an oxide shell.

The same ensemble of nanoparticles following complete oxidation into Fe_3O_4 is shown in figure 1(c), where we observe the disappearance of Ashby-Brown contrast, and each nanoparticle possesses uniform contrast. The evolution of diffraction contrast is indicative of a structural or compositional change, as adherence to the carbon substrate precludes any rotational or translational movement. From the introduction of O_2 gas and increasing temperature we observed appreciable drift in the ensemble which is indicated by the single nanoparticle in red (figures 1(a) and (c)).

The conversion of FeO@Fe_3O_4 core–shell nanoparticles to pure Fe_3O_4 nanoparticles is confirmed by SAD pattern in figure 1(d). Following complete oxidation of the nanoparticle ensemble (t_f), there is an increase of the brightness of the Fe_3O_4 (220) reflection as well as the disappearance of the FeO (220) reflection and emergence of the (422), (522), and (440) reflections of Fe_3O_4. While there are enough differences in the SAD patterns from the ensemble to discern between FeO and Fe_3O_4, this becomes much more difficult on the single particle level, as the main reflections for FeO and Fe_3O_4 can overlap depending on the nanoparticle zone axis. However, at the single particle level the diffraction contrast can provide a unique pathway to identify a structural or compositional transformation *in-situ*, and in real time. We therefore tracked a single nanoparticle that showed Ashby-Brown contrast at t_0 through to complete oxidation at t_f. We used GMS to down-select a region of interest of the *in-situ* dataset, to align and track the

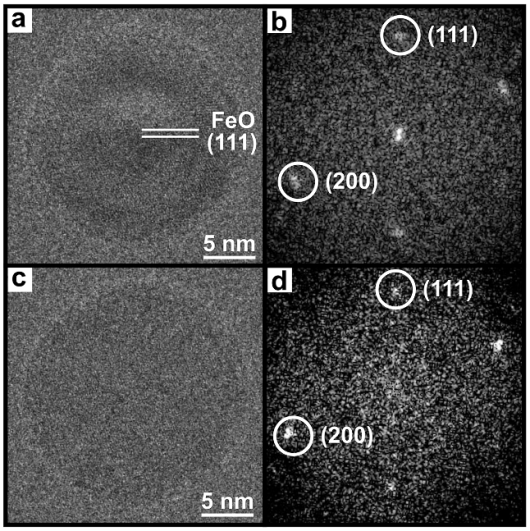

Figure 2. TEM (a) and corresponding FFT (b) images of a single FeO@Fe_3O_4 core–shell nanoparticles taken at t_0. From (b) the particle is oriented along the [110] direction, with a slight tilt observed due to the non-uniform brightness of the spots. The alternating light and dark contrast observed in (a) is positioned perpendicular to the strongest (111) reflection. TEM (c) and corresponding FFT (d) images of a magnetite nanoparticles taken at t_f.

single FeO@Fe_3O_4 nanoparticle highlighted in red in figure 1. The complete *in-situ* transformation is given as a video in supporting information, video S1.

Figure 2(a) shows the down selected FeO@Fe_3O_4 core–shell nanoparticle taken at t_0, along with the corresponding fast Fourier transform (FFT) in figure 2(b). The nanoparticle shows alternating light and dark diffraction contrast perpendicular to the (111) diffraction spot, indicating (111) is the principal diffracting plane causing the contrast. From FFT analysis the nanoparticle is oriented along the [110] zone axis. There appears to be a slight tilt due to the non-uniform brightness of the (111) spots in the FFT. Figure 2(c) shows a TEM image of the same nanoparticle now fully oxidized to Fe_3O_4 at t_f, with the corresponding FFT in figure 2(d) indicating no change in crystallographic orientation following oxidation. However, the alternating light and dark contrast has evolved into uniform contrast across the nanoparticle. To track the evolution of the light and dark contrast over time, snapshots of the *in-situ* video at various time points were taken corresponding to the most striking changes in particle appearance. Figure 3(a) shows the FeO@Fe_3O_4 nanoparticle taken at $t = 23$ s, with figures 3(c), (e) and (g) showing nanoparticles at varying stages of oxidation taken at $t = 96$ s, $t = 100$ s, and $t = 148$ s, respectively. To quantify the change in diffraction contrast we summed the pixel intensity profiles across the white highlighted areas which are perpendicular to the direction of the alternating contrast (along the [111] direction of the dominant reflection), with the profiles given alongside the respective TEM image. In figure 3(a), the nanoparticle at $t = 23$ s shows an alternating dark and light contrast, which is represented in figure 3(b) as a pseudo-sinusoidal intensity profile. For the nanoparticle at $t = 96$ s, the diffraction contrast in figure 3(e) is somewhat flatter, with the profile intensity in figure 3(f) likewise reduced along with a change in peak position. At $t = 100$ s (figure 3(i)) we again observe alternating light and dark contrast. However, the peak position has now shifted when compared to the initial nanoparticle and the diffraction contrast intensity profile is inverted (figure 3(j)). We also observe an additional third peak of contrast emerge. Finally, after complete oxidation at $t = 148$ s we observe uniform contrast in the nanoparticle (figure 3(m)), which is confirmed in the extracted intensity profile (figure 3(n)). Such an evolution of diffraction contrast was reported by Ashby and Brown [10]. They showed that a small spherical inclusion contained within a matrix with coherent strain displays alternating contrast directed perpendicular to a line of no contrast. Further, they showed that the diffraction contrast displayed is dependent on the size of the inclusion, its shape, and its depth in the matrix with respect to the upper surface. It was also theorized that as the inclusion increased its depth with respect to the foil surface, the contrast profile would evolve and invert in both bright and dark field conditions.

To understand the structural contribution to the change in diffraction contrast we made a qualitative comparison to simulations of TEM images of model FeO@Fe_3O_4 core–shell nanoparticles with changing core sizes. Models were formed with a FeO@Fe_3O_4 core–shell structure containing different core size and shell thickness. To simulate a change in the depth of the inclusion the core was offset within the shell to create uniform, low-skew, and high-skew core–shell structures (figure S4). The systems were relaxed and then heated to 300 K in the canonical ensemble (NVT) over 10 000 steps and quenched using the conjugate

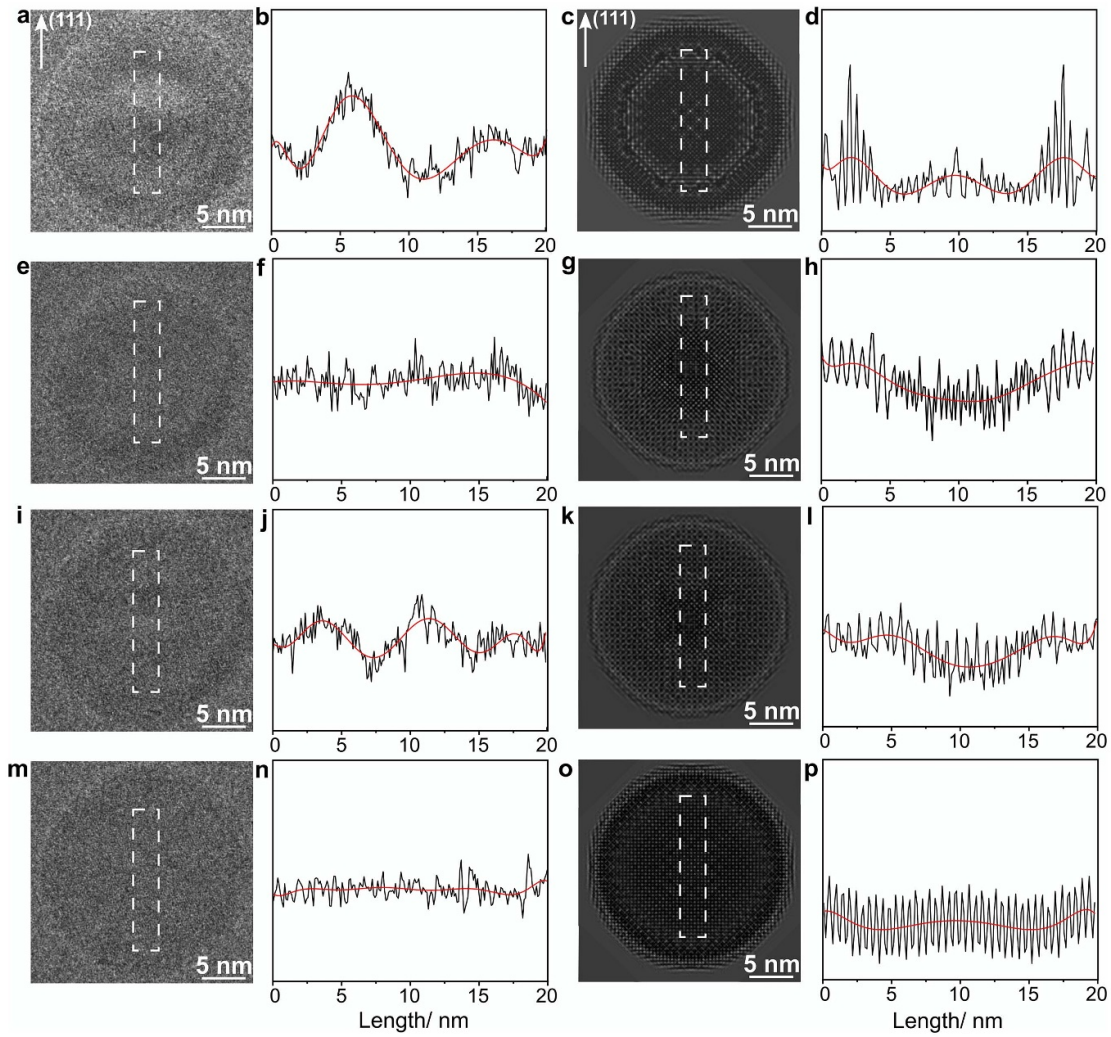

Figure 3. TEM images (a), (e), (i), (m) and JEMS simulated (c), (g), (k), (o) images of an individual FeO@Fe_3O_4 nanoparticles oriented along [001] and corresponding contrast profiles taken by summing the pixel intensity within the white box. (a)–(d) correspond to the FeO@Fe_3O_4 nanoparticle at $t = 23$ s, (e)–(h) at $t = 96$ s, (i)–(l) at $t = 100$ s, and (m)–(p) a fully oxidized Fe_3O_4 nanoparticle at $t = 148$ s.

gradient method to attain the zero-force configuration, using a timestep of 1 fs to run the calculations. The open source LAMMPS software was used to run the simulations [24]. Then, atomic resolution phase contrast image simulations were carried out using the algorithm within the JEMS program. The atomic models were viewed down the [110] direction (figure S5) and simulated in JEMS to compare directly to experiment. The contrast intensity profiles of the simulated HRTEM images from the atomic models show a similar pattern as the intensity profiles obtained from the *in-situ* experiment. The intensity profile of the uniform core–shell model (figure 3(d)) possesses the same pseudo-sinusoidal profile comparable to the intensity profile of the experimental TEM image (figure 3(b)). The intensity and phase of the peaks differs, however exactly matching the size and depth of the FeO core between simulation and experiment is not possible. In figure 3(h) the profile of the low-skew model flattens, mimicking the behavior seen at $t = 23$ s in experiment. The profile intensity of the high-skew simulation is given in figure 3(l), and shows an inversion of the contrast intensity profile when compared to figure 3(d) which again matches the experimental profile change at $t = 96$ s. Finally, a simulation of a single crystal Fe_3O_4 nanoparticle (figure 4(p)) displays a uniform contrast profile which is similar to the intensity profile of the experimental TEM image (figure 4(n)).

As the shape and symmetry of Ashby-Brown contrast in bright-field images depends on the depth of the inclusion in the upper surface of the foil, and contrast symmetry only occurs in bright-field images when the inclusion is at center height, these results would indicate that the shell is not oxidizing uniformly. Further, the inversion of alternating light and dark contrast bands indicates that at $t = 96$ s the inclusion is towards the lower surface of the matrix, as observed by Ashby and Brown [10]. In our case, this arises from asymmetric oxidation due to the deposition of FeO@Fe_3O_4 nanoparticles onto the carbon substrate, as illustrated in

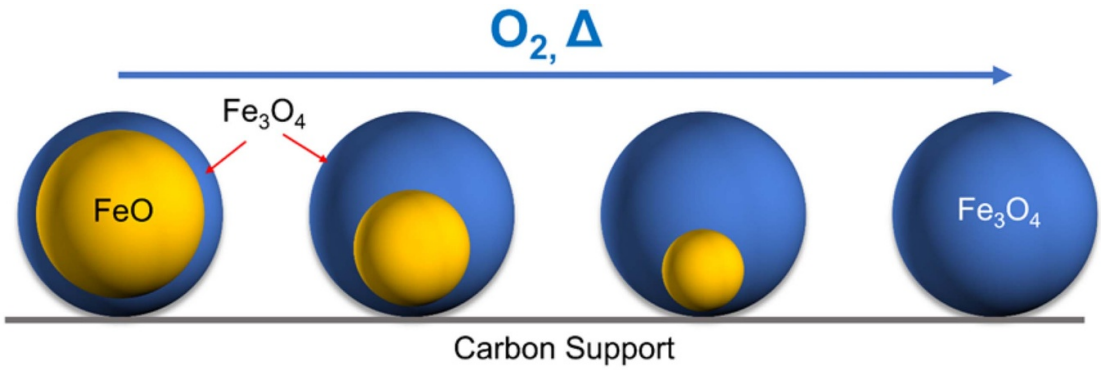

Figure 4. FeO@Fe_3O_4 core–shell nanoparticle undergo asymmetric oxidation in an *in-situ* TEM experiment. The carbon support limits oxidation occurring from the lower side of the nanoparticle. This means the FeO core can be considered an inclusion that reduces in size, and increases in depth, from the surface of the Fe_3O_4 shell.

figure 4. Oxygen gas flows across the upper surface of the nanoparticles and oxidizes the nanoparticles from the top-down.

It has previously been shown that a single line of no contrast flanked by two lobes of contrast was indicative of a fully coherent and symmetrical strain field across the interface, whereas multiple contrast lines suggested the presence of misfit dislocations and the loss of coherency [25]. However, the nanoparticles used in this study have an average size of 21.1 nm which is not expected to be large enough to support misfit dislocations. The thickness of a pseudomorphic layer of magnetite on a substrate of wustite is at least 16 nm, indicating a larger nanoparticle diameter would be needed for misfit dislocations to emerge [26]. In fact, in a uniform thin film particles as large as 35 nm in diameter appear to possess coherent strain fields [11, 23]. However, if the foil matrix was deformed by 5% in tension the characteristic contrast of a coherent strain field was lost, and multiple lines of no contrast were observed [11]. Core–shell nanoparticles possess considerable tensile strain at their interface, with extended facets showing increased tension compared to corner or edge sites [27, 28]. In a spherical inclusion the strain is expected to be relatively uniform throughout the interface, however it will increase with increasing curvature i.e. decreasing core size. This is observed in figure 3(j); the contrast has inverted when compared to figure 3(b) indicating the FeO core position has moved downwards with respect to the upper Fe_3O_4 nanoparticle surface, and the number of contrast bands has increased indicating an increase in strain due to the smaller core size.

4. Conclusion

In conclusion, our study demonstrates that diffraction contrast can be used as a simple approach to monitor the structural and compositional evolution of nanoparticles, as shown by tracking the complete oxidation of FeO@Fe_3O_4 core–shell nanoparticles to single crystal Fe_3O_4 nanoparticles. The distinct light and dark contrast observed at the center of the nanoparticles corresponds to the characteristic 'Ashby-Brown' contrast, indicating the presence of a FeO@Fe_3O_4 core–shell structure. As the nanoparticles undergo oxidation under flowing O_2 gas in an *in-situ* TEM the contrast profile evolves, inverts and then gradually disappears, indicating the transformation into single-crystal Fe_3O_4. This concept presents a new pathway to identify and track oxidation or reduction of nanoparticles without relying on high-resolution TEM, scanning transmission electron microscopy (STEM), or EELS spectral imaging.

Data availability statement

The data that support the findings of this study are available upon reasonable request from the authors.

Acknowledgments

This work was supported by the Laboratory Directed Research and Development (LDRD) program of Los Alamos National Laboratory under Project No. 20210604ECR and the LDRD program at Sandia National Laboratories. This work was performed, in part, at the Center for Integrated Nanotechnologies (CINT), an Office of Science User Facility operated for the US Department of Energy (DOE) Office of Science. Los Alamos National Laboratory, an affirmative action equal opportunity employer, is managed by Triad National Security, LLC for the U.S. Department of Energy's NNSA, under contract 89233218CNA000001.

Sandia National Laboratories is a multimission laboratory managed and operated by National Technology & Engineering Solutions of Sandia, LLC, a wholly owned subsidiary of Honeywell International, Inc., for the US DOE's National Nuclear Security Administration under contract DE-NA-0003525. The views expressed in the article do not necessarily represent the views of the U.S. DOE or the United States Government. The use of the K3 IS camera at CINT was provided courtesy of Gatan. R K would like to acknowledge the support by National Science Foundation, Future Manufacturing Program, Award 2240407. LA-UR-23-26777.

ORCID iDs

Dale L Huber https://orcid.org/0000-0001-6872-8469
John Watt https://orcid.org/0000-0002-8012-9837

References

[1] Alcorn F M, Jain P K and van der Veen R M 2023 Time-resolved transmission electron microscopy for nanoscale chemical dynamics *Nat. Rev. Chem.* **7** 256–72
[2] He B W, Zhang Y X, Liu X and Chen L W 2020 *In-situ* transmission electron microscope techniques for heterogeneous catalysis *Chemcatchem* **12** 1853–72
[3] Jinschek J R 2014 Advances in the environmental transmission electron microscope (ETEM) for nanoscale *in situ* studies of gas-solid interactions *Chem. Commun.* **50** 2696–706
[4] Liu X, Zhang C H, Li Y W, Niemantsverdriet J W, Wagner J B and Hansen T W 2017 Environmental transmission electron microscopy (ETEM) studies of single iron nanoparticle carburization in synthesis gas *ACS Catal* **7** 4867–75
[5] Levin B D A 2021 Direct detectors and their applications in electron microscopy for materials science *J. Phys. Mater.* **4** 042005
[6] Murthy A A, Stanev T K, Dos Reis R, Hao S, Wolverton C, Stern N P and Dravid V P 2020 Direct visualization of electric-field-induced structural dynamics in monolayer transition metal dichalcogenides *ACS Nano* **14** 1569–76
[7] Poerwoprajitno A R, Gloag L, Watt J, Cheong S, Miller B K, Huber D L and Tilley R D 2022 *In-situ* ETEM reveals formation mechanism of single Pt atom on Ru nanoparticle electrocatalysts for CO-resilient methanol oxidation *Microsc. Microanal.* **28** 130–1
[8] Poerwoprajitno A R *et al* 2022 A single-Pt-atom-on-Ru-nanoparticle electrocatalyst for CO-resilient methanol oxidation *Nat. Catal.* **5** 231–7
[9] Singh M K, Ghosh C, Miller B, Kotula P G, Tripathi S, Watt J, Bakan G, Silva H and Carter C B 2020 *In situ* TEM study of crystallization and chemical changes in an oxidized uncapped $Ge_2Sb_2Te_5$ film *J. Appl. Phys.* **128** 124505
[10] Ashby M F and Brown L M 1963 Diffraction contrast from spherically symmetrical coherency strains *Phil. Mag.* **8** 1083–103
[11] Phillips V A and Livingston J D 1962 Direct observation of coherency strains in a copper-cobalt alloy *Phil. Mag.* **7** 969–80
[12] Williams D B and Carter C B 2009 *Transmission Electron Microscopy: A Textbook for Materials Science* ed D B Williams and C B Carter (Springer) pp 463–81
[13] Christodoulou S *et al* 2015 Band structure engineering via piezoelectric fields in strained anisotropic CdSe/CdS nanocrystals *Nat. Commun.* **6** 7905
[14] Kim D Y, Choi K W, Zhong X L, Li Z Y, Im S H and Park O O 2013 Au@Pd core-shell nanocubes with finely-controlled sizes *Crystengcomm* **15** 3385–91
[15] Chen Z Y, Chou K C and Morita K 2016 Mechanism of metastable wustite formation in the reduction process of iron oxide below 570 degrees C *Mater. Trans.* **57** 1660–3
[16] Wetterskog E, Tai C W, Grins J, Bergstrom L and Salazar-Alvarez G 2013 Anomalous magnetic properties of nanoparticles arising from defect structures: topotaxial oxidation of $Fe_{(1-x)}O|Fe_{(3-delta)}O_4$ core|shell nanocubes to single-phase particles *ACS Nano* **7** 7132–44
[17] Nedelkoski Z *et al* 2017 Origin of reduced magnetization and domain formation in small magnetite nanoparticles *Sci. Rep.* **7** 45997
[18] Vreeland E C *et al* 2015 Enhanced nanoparticle size control by extending LaMer's mechanism *Chem. Mater.* **27** 6059–66
[19] van Duin A C T, Dasgupta S, Lorant F and Goddard W A 2001 ReaxFF: a reactive force field for hydrocarbons *J. Phys. Chem.* A **105** 9396–409
[20] Aryanpour M, van Duin A C and Kubicki J D 2010 Development of a reactive force field for iron-oxyhydroxide systems *J. Phys. Chem.* A **114** 6298–307
[21] Perdew J P, Burke K and Ernzerhof M 1996 Generalized gradient approximation made simple *Phys. Rev. Lett.* **77** 3865–8
[22] Stadelmann P Java-EMS (JEMS) program; software (available at: www.jems-swiss.ch/Home/jemsWebSite/jems)
[23] Ashby M F and Brown L M 1963 On diffraction contrast from inclusions *Phil. Mag.* **8** 1649–76
[24] Thompson A P *et al* 2022 LAMMPS—a flexible simulation tool for particle-based materials modeling at the atomic, meso, and continuum scales *Comput. Phys. Commun.* **271** 108171
[25] Song L L, Liu S and Mao X 2017 A new method for fast statistical measurement of interfacial misfit strain around nano-scale semi-coherent particles *RSC Adv.* **7** 28506–12
[26] Matthews J W and Blakeslee A E 1974 Defects in epitaxial multilayers: i. Misfit dislocations *J. Cryst. Growth* **27** 118–25
[27] Liu M X *et al* 2021 Core-shell nanoparticles with tensile strain enable highly efficient electrochemical ethanol oxidation *J. Mater. Chem.* A **9** 15373–80
[28] Nathanson M, Kanhaiya K, Pryor A Jr, Miao J and Heinz H 2018 Atomic-scale structure and stress release mechanism in core-shell nanoparticles *ACS Nano* **12** 12296–304